Nonequillibrium Green's function analysis of interwell transport and scattering in monopolar lasers

Xin Zheng,[1] Wanqiang Chen,[1] Michael Stroscio,[2] and Leonard F. Register[1]
[1]*Microelectronic Research Center, Department of Electrical and Computer Engineering, The University of Texas at Austin, Austin, Texas 78758, USA*
[2]*Department of Electrical and Computer Engineering and Department of Physics, University of Illinois at Chicago, Chicago, Illinois 60607-7053, USA*
(Received 9 September 2005; published 5 June 2006)

Transport and scattering is examined in a simple coupled double-well model of infrared monopolar lasers via a nonequilibrium Green's function (NEGF) based analysis. Roughly speaking, in such lasers a more or less three level system is formed where electrons are injected into the first excited state subband of a leading well, decay via photon emission to intermediate ideally resonant-state subbands resulting from coupling of the ground state subband of the leading well to the first excited state subband of the trailing well, and subsequently, preferably quickly to allow population inversion between the initial and intermediate state, decay via phonon emission to the ground state subband of the trailing well. Golden Rule based analysis is widely used to model scattering including in this system. Implicit in its use is a random-phase approximation among the final states. However when scattering processes appear to produce not only changes in energy states but also real-space transport as between the wells here, this approximation can become suspect. In this work the affects of this approximation on scattering-induced population and depopulation of intermediate level(s) are addressed and overcome using a NEGF technique that allows consideration of transport and scattering absent the Golden Rule and associated random phase approxmiations. It is found that as the barrier becomes thick, the Golden Rule approximation can overestimate the depopulation rate of the intermediate levels. Through changes in the homogeneous broadening of the photon transition associated with changes in the depopulation rates of the intermediate level(s), the variations in barrier thickness could also have additional effects on population inversion and gain not apparent through Golden Rule calculations. Accordingly, barrier thickness is found to also be a potentially critical parameter for optimizing device performance.

DOI: 10.1103/PhysRevB.73.245304 PACS number(s): 73.21.Fg, 73.63.Hs

I. INTRODUCTION

Intersubband injection lasers operate on the condition that phonon-assisted interwell electronic transitions provide a fast depopulation of the final states of the optical transition allowing population inversion.[1] Although both cascaded and noncascaded designs have been successfully implemented, the essential element, two quantum wells separated by a tunnel barrier, is the same, as illustrated in Fig. 1. To optimize the carrier transport through the barrier, the quantum wells are designed such that the lower subband of leading quantum well (the narrower of the two quantum wells in the exampled of Fig. 1) and the first excited subband of the trailing quantum well (the wider well in the example of Fig. 1) are nominally degenerate allowing for coherent quantum mechanical tunneling between wells; to optimize phonon scattering the energy separation between the ground and excited state of the trailing well are tuned according to the phonon energies.[2–9] Previously, Golden Rule (GR) based calculations have been used to carefully examine the effects of variations in the well widths and of the various types of phonon modes involved, interface and confined, on this process.[10] In this work, nonequilibrium Green's function (NEFG) based calculations with scattering are used to extend this study by examining the essential effects of variation of the barrier thickness.

The indicated switch from a GR-based analysis to a true quantum transport calculation is inherently necessary to achieve the above goal over the full range of barrier thicknesses considered (although the use of simpler models may be possible in various limiting cases), and demonstrating and explaining this need is a secondary goal of this work. Under the ideal resonance condition, the energy eigenstates associated with the ground subband of the first well and the first excited subband of the second well are, in fact, delocalized among the two wells, a result that is independent of the barrier thickness even if harder to achieve for thicker barriers. Under these conditions the GR calculation neglects the time required for coherent tunneling between the wells via the implicit application of the random phase approximation (RPA) among the intermediate states, as is elaborated on in the Results. This is a reasonable approximation for sufficiently thin barriers. However, as the barrier becomes thicker, the interwell tunneling time will become a significant and then the dominant limitation on depopulation of the final state of the optical transition.

II. SCHRÖDINGER EQUATION MONTE CARLO

In this work these quantum *transport* issues are addressed using the unique nonequilibrium Green's function code Schrödinger Equation Monte Carlo (SEMC).[11] SEMC already has been used to study the effects of phase-coherence and phase-breaking on carrier capture by quantum wells,[11–14] and failures of the Golden Rule to properly model carrier capture in tunnel injection lasers[14] among other things.

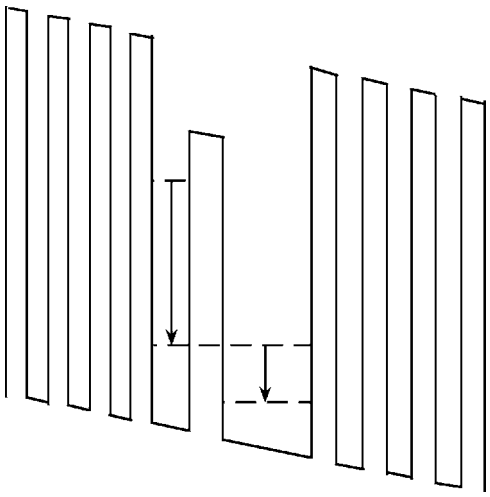

FIG. 1. A typical quantum-well laser structure. The left arrow shows the optical emission and the right arrow shows the phonon emission.

SEMC provides a qualitatively and quantitatively accurate, nonperturbative, current conserving treatment of coherent electron transport and phonon-mediated transport due to real scattering processes, including the process of long-range polar-optical phonon scattering considered here. The "Schrödinger Equation Monte Carlo" moniker was chosen as an indicator of the unique Monte Carlo based method of treating phase-breaking scattering, while coherent propagation of the complex wave function continues to be treated deterministically. The SEMC method is described in detail in Ref. 11; a brief summary is provided here.

Scattering and the associated phase breaking and energy dissipation within this Schrödinger equation-based method are modeled via the exchange of probability among oscillator degrees of freedom n_q within a many-body electron-phonon system just as in the true carrier-phonon scattering. A set of Schrödinger equations is defined for the charge carrier corresponding to an "initial" state $\psi(\mathbf{r},n_1,\ldots,n_q,\ldots,n_Q)$ and many (e.g., 100s or 1000s of) "final" states separated from the initial state by the emission or absorption of one phonon $\psi(\mathbf{r},n_1,\ldots,n_q\pm 1,\ldots,n_Q)$. Coupling potentials between the initial and final states are provided by Monte Carlo sampling of the (spatial correlation functions of the) true carrier-phonon interactions (for phonons of approximately the same energy) $M(\mathbf{r},q)$. A probability source (which makes this a Green's function method as noted) to the initial state $A(\mathbf{r},E)$ (capital Greek "alpha" for 'the beginning') is provided by an open boundary in the carrier coordinates or coupling to the prior phonon state, or *as for the calculations of this work* and that of Ref. 15, *a prior photon state*; probability sinks $\Omega(\mathbf{r},E)$ ("Ω" for the "the end") are provided by open boundaries in the carrier coordinates of both the initial and final states and/or, as required for bound final states in this work, complex "self-energy" potentials in the final states representing still subsequent scattering. The equation (or set of equations, depending on how you look at it) to be solved (simultaneously) is of the basic form,

$$[H_e(\mathbf{r})-E+\Omega(\mathbf{r},E)]\psi(\mathbf{r},n_1,\ldots,n_q,\ldots,n_Q)+\sum_{\pm}\sum_{q=1}^{Q}M(\mathbf{r},q)\sqrt{n_q+\frac{1}{2}\pm\frac{1}{2}}\psi(\mathbf{r},n_1,\ldots,n_q\pm 1,\ldots,n_Q)=A(\mathbf{r},E)$$

for the "initial" state and

$$[H_e(\mathbf{r})-(E\mp\hbar\omega_q)+\Omega(\mathbf{r},E\mp\hbar\omega_q)]\psi(\mathbf{r},n_1,\ldots,n_q\pm 1,\ldots,n_Q)+M(\mathbf{r},q)\sqrt{n_q+\frac{1}{2}\pm\frac{1}{2}}\psi(\mathbf{r},n_1,\ldots,n_q,\ldots,n_Q)=0$$

for the "final" states. (This basic equation is then transformed into the most convenient coordinates system, specifically the real-space coordinate x normal to the plane of the wells and the crystal momentum coordinate $\mathbf{k}_{y,z}$ in the plane of the wells in this case.) This equation is solved to find the many-body carrier-phonon wave functions $\psi(\mathbf{r},n_1,\ldots,n_Q)$ from which any physical observable (transmission, reflection, and capture probabilities, self-energies/scattering rates, currents in real-space or "phonon-space," etc.) can be obtained. Probability and energy are inherently conserved and phase information is inherently retained with respect to the full-many body system, but with respect to the carrier alone, the interaction is inelastic and phase breaking although still probability conserving.

This procedure precisely emulates scattering, both real and virtual, in the true carrier-phonon system to first-order, and to higher orders within the accuracy of the estimated final-state self-energies. Scattering is neither local in position nor time. Indeed, the calculations of this work are time-independent propagating energy eigenstate calculations in the coupled carrier-phonon system. "Initial" and "final" only indicates the direction of probability current flow in the phonon coordinates.

This basic procedure can be repeated sequentially to trace carriers through an unlimited number of scattering "events." The old initial state becomes the source; a new intermediate state is selected by Monte Carlo sampling from among the old final states according to the probability flow to/through the final states, and a new set of final states is generated each with its own complex self-energy potentials.

III. DEVICE MODEL

To isolate the essential physics we have used the basic square-well potential structure, if not precise numerical values, that was used previously in the GR-based analysis of this system, Ref. 10, as shown in Fig. 2 for one particular set of well and barrier widths. We have also used an envelope function approximation for the electrons and the macroscopic model of the phonon modes employed in Ref. 10. The electron effective masses and nonparabolicity constants for the well and barrier materials, and the parameters used to calculate the confined, interface and half-space phonon modes and their interaction with electrons in SEMC are given in Table I. Note that in actual intersubband lasers,

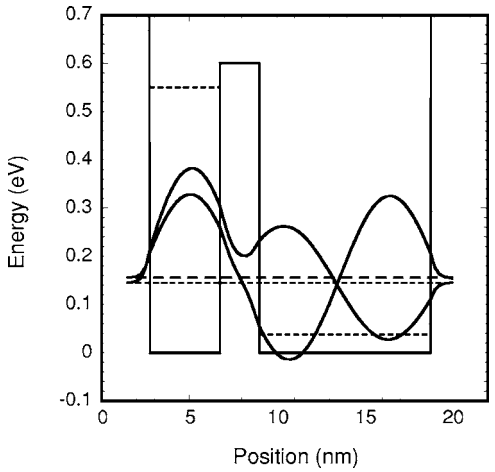

FIG. 2. Band diagram and energy levels of an AlAs/GaAs double quantum well heterostructure. Here, the ground state of the first well is aligned with the first excited state of the second (in the limit of large barrier thicknesses) to maximize interwell tunneling. The two delocalized energy eigenfunctions resulting from this alignment are also shown (with the zero reference for the each eigenfunction aligned to its respective energy eigenvalue).

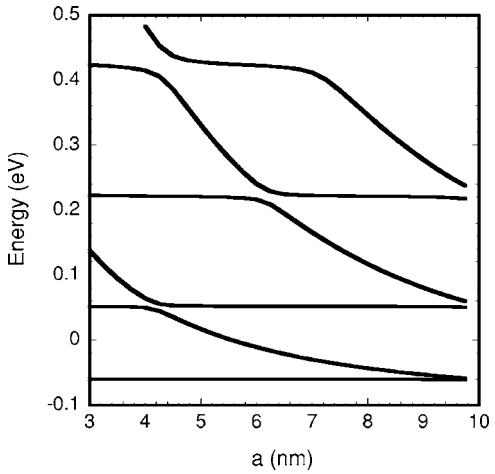

FIG. 3. Subbands in the double-well structure as a function of a, the first well width, for fixed barrier width (2 nm) and second well width (10 nm). Except near the anticrossings, the width-dependent energies are of course those of states localized predominately to the first well, and the width independent energies those of state localized predominately to the second well.

whatever the actual well widths discretized in terms of atomic layers, resonance between the wells is achieved through adjustment of the potential drop across the device, as illustrated in Fig. 1. In the square-well model system of Ref. 10, for modeling purposes it was achieved through adjusting the well widths continuously. Here, subject to the constraints of a discrete lattice required for the SEMC calculations, once the system was near resonance, the dept of the first well was adjusted to fine tune the resonance when required to retain (by choice not necessity) the square-well nature of the model.

We injected carriers, actually a carrier probability current, into the simulation region via photon emission using the usual electron photon interaction Hamiltoninan $H \propto (n_{\text{photon}}+1)\hat{\mathbf{A}}\cdot\mathbf{p}$ operating on the well-localized excited state wave function of the first well to define the source term $A(\mathbf{r},E)$, where $\hat{\mathbf{A}}$ is a unit vector in the direction of the vector potential which is assumed to be normal to plane of the well here, $\mathbf{p}$ is the momentum operator operating on the electron coordinate, and n_{photon} is the photon occupation number representing the, here arbitrary, intensity of the light. The energy E in the above equations and here is the excited state energy of the first well minus the photon energy $\hbar\omega_{\text{photon}}$. To isolate the essential physics we have taken the 0 K temperature limit so that the only way out of the first well in these simulations is, roughly speaking, via tunneling through the barrier and down to the ground subband of the second well via phonon emission where the probability current is then absorbed via a complex potentials $\Omega(\mathbf{r},n_1,\ldots,n_q-1,\ldots,n_Q)$ representing subsequent scattering as described in Sec. II.

Of course other scattering mechanisms, such as acoustic phonon scattering, carrier-carrier scattering, interface roughness scattering, impurity scattering etc. could aid in the depopulation of the final state of the optical transition. However, the essential limitation of the GR-based calculations for these processes would be the same. On the other hand, when the wells are not in resonance and the intermediated states become much more localized to one well or the other, the artifacts of GR calculations considered in this work would be at least reduced. However, under this latter condition, the depopulation rate would be less than optimal and the interwell transitions themselves would likely mediated by the various scattering processes (which is actually included in the calculations here for optical phonon emission). Our goal in this work is to isolate and address the essential physics of the optimal processes intended by design.

IV. SIMULATION RESULTS

The energy states within two wells as a function of the first well width a are shown in Fig. 3, for the specific case of a 2 nm barrier and the second well of 10 nm width. The resonance between the ground state in the first well and the

TABLE I. Effective mass, nonparabolicity constant, dielectric constant, and phonon frequencies used in this work (Ref. 16).

	M^*	Nonparabolicity	ε(high)	ε(low)	ω(LO)/meV	ω(TO)/meV
GaAs	0.067	0.61	12.90	10.89	36.25	33.29
AlAs	0.14	0.25	8.15	10.90	50.09	44.88

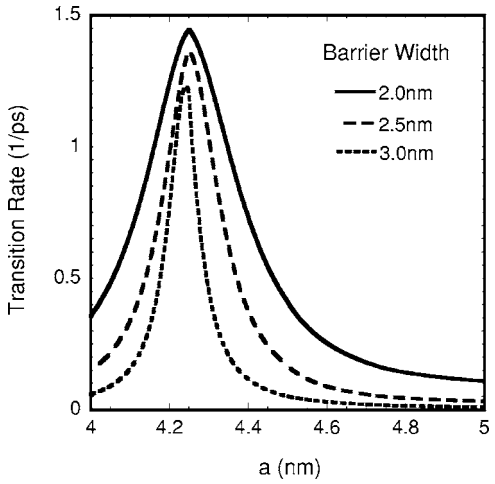

FIG. 4. Interwell polar optical-phonon-assisted transition rate under the double electron-phonon resonance condition as a function of a, width of the first well, with the second well width fixed at 10 nm. As the barrier becomes thicker, not only does the resonance width decrease but the peak transition rate decreases as well.

first excited state in the second well occurs at $a=4.25$ nm where the anticrossing is found. Or at least it does so to within the spatial resolution of the code; again a small adjustment to the potential in the first well was made to optimize the resonance at this point.

The transition rates from the intermediate state after photon emission in the first well to the final, ground state localized to the second well—calculated as the probability current flow out of the intermediate state divided by the probability density in the intermediated state—are showin in Fig. 4 as a function of the width of the first well. For this figure and Fig. 5 the photon energy is chosen as that for which the injection current is greatest, which as expected is roughly the energy separation between what would be the well-defined ground and first-excited states of the first well in the absence of the

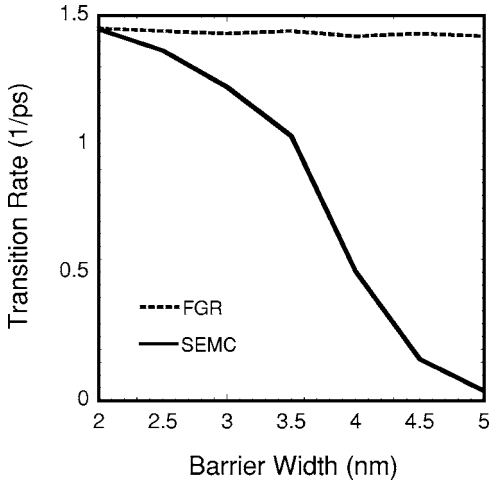

FIG. 5. Maximum transition rate, occurring at the anticrossing, as a function of barrier width for SEMC and GR calculations. Note that the GR results are essentially unaffectted by the barrier width while for SEMC calculations the transition rate falls as tunneling becomes the limiting process.

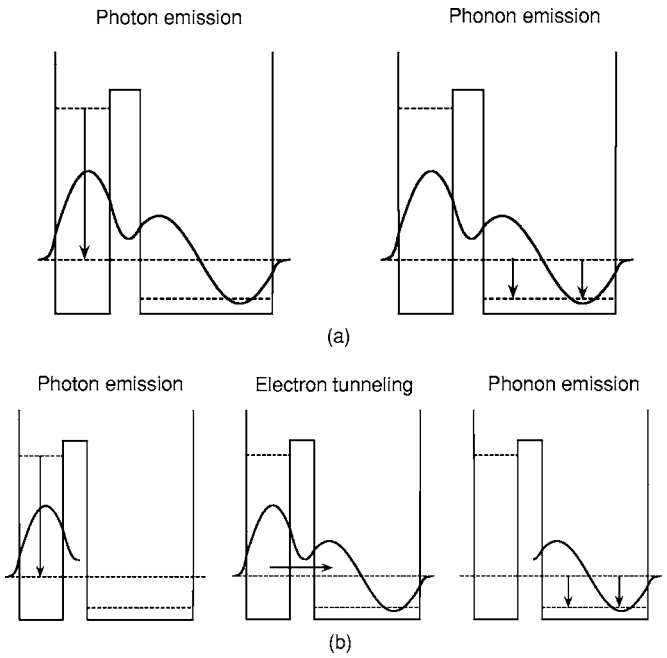

FIG. 6. Illustration of physical processes considered via the GR assumption, and via SEMC. (a) In GR calculations only two physical processes are considered: photon emission to one of the two delocalized intermediate state is followed directly by the phonon emission from that the intermediate state to the final state localized in the second well. (b) SEMC addresses three physical processes: photon emission, real-space transport/tunneling through the barrier and phonon emission.

tunneling and scattering that broaden these states in SEMC. In this calculation, both interface and confined phonon modes are considered as in Ref. 10. Our results for the 2 nm barrier show a close coincidence (both in shape and peak of the curve) with the result obtained in the GR-based calculations of Ref. 10. As expected, the total transition process, photon emission followed by phonon emission, from the excited state localized to the first well to the ground state localized to the second well is optimized at this anticrossing where the intermediate states—the final state for the optical transition and the initial state for phonon scattering—are delocalized among the two wells. For GR calculations, however, this is simply because the intermediate state wave functions significantly overlap both the initial and final states. There is no direct consideration of the tunneling time. As a result, at the anticrossing, the GR calculations simply saturate for large well thicknesses as shown in Fig. 5.

However, also as shown in Fig. 5, as the barrier width increases the corresponding transistion rate decreases rapidly in the SEMC calculations. At a 2 nm barrier width, the GR and SEMC give nearly the same results, while by time the barrier thickness goes to 5 nm, the SEMC calculations give a transition rate of approximately 3% of that obtained via the GR approximation. The reason for the discrepancy is, again, that tunneling through the interwell barrier limits the depopulation rate of the intermediate state. Roughly speaking, for thick barriers at least, there are three processes to consider each of which takes time, as illustrated in Fig. 6(b) and shown via the SEMC simulation of Fig. 7. Photon emission

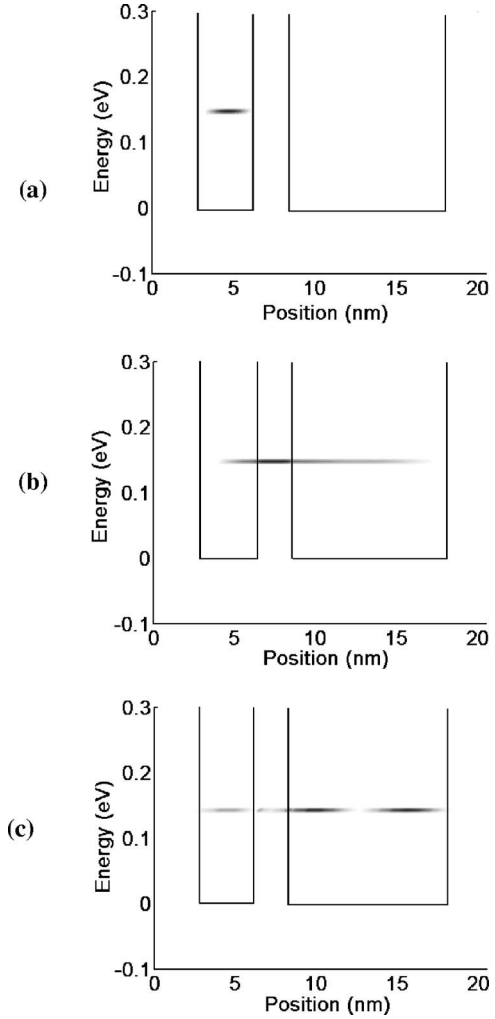

FIG. 7. Current flow in the double-quantum-well laser given by SEMC simulation for fixed photon energy as a function of the intermediate state energy and position for a 2 nm barrier, with darker areas indicating greater current flow: (a) probability flow into the intermediate state due to photon emission, (b) real-space probability current flow to the right after photon emission and before phonon emission, and (c) probability flow out of the intermediate state energy state due to phonon emission. Solid lines represent the well potential structure (at $\mathbf{k}_{\|}=0$). The nonzero energy widths of these contours and the residual phonon emission within the first well seen in (c) result from the homogeneous broadening of the electron states.

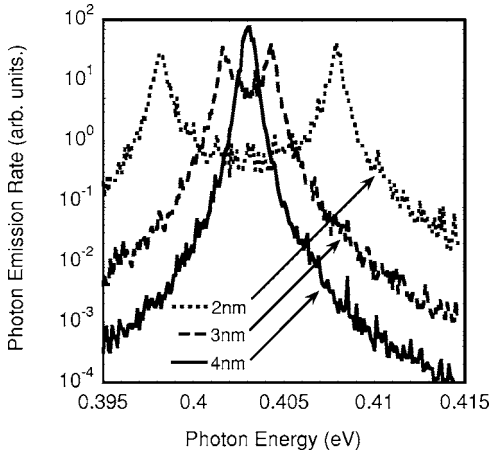

FIG. 8. Rate of photon emission as a function of photon energy (arbitrary units) for different barrier widths. The noise in the figure is a result of the Monte Carlo technique used to model scattering. Note that when the barrier is thin and the wells strongly coupled and phonon emission limits the transition rate out of the intermediate states (2 and 3 nm well widths; see Fig. 5), two intermediate states of almost barrier-width-independent amplitude and width are well resolved. However, when the barrier becomes thicker and tunneling begins to limit the transition rate (4 nm well width), the two states overlap and the phonon emission peak becomes narrower and stronger at the peak with the decreasing broadening of the intermediate state.

first takes the electron to one or the other or, particularly for thicker barriers, a coherent overlap of the two roughly degenerate states at the anticrossing that is *localized to the first well*. The electron then propagates to the second well via tunneling (roughly in a time commensurate with the energy level splitting). Then finally, the electron now within the second well emits a phonon to be captured in the ground state that is localized to the second well. Of course in reality, and in SEMC, these individual processes are not so well separated. In contrast, the random-phase approximation among energy eigenstates implicit to the GR—GR calculations provide the squares of the magnitudes of the amplitude coefficients of the eigenstates only, ignoring any coherence between differing initial and/or differing final states—places carriers in an incoherent overlap of the intermediate states which, as a result, already overlaps the second well in position immediately after "completion" of the photon emission regardless of barrier thickness. As a result the three-step process of Fig. 6(b) is artificially turned into a two-step process, as illustrated in Fig. 6(a); the time to tunnel through the barrier is it not considered regardless of the barrier thickness. The fallacy of this latter result is self-evident if one considers huge wells separations of, e.g., a micron, but it becomes important at only a few nanometers as shown by Fig. 5. This neglect of the time required for real-space transport is a common failure mode for the GR approximation when initial and final states are not localized to the same region.[11,14]

In addition to affecting the transition rate between wells, the barrier thickness affects the photon emission rate as well, as shown in Fig. 8. As the thinner barrier leads to an increased depopulation rate for the intermediate states, it also inherently leads to an increase in homogeneous (energy/collision/finite-lifetime) broadening of the photon transition to the intermediate states. This homogeneous broadening, in turn reduces the peak photon emission rate per electron in the excited state of the first well, a peak that would be aligned to the lasing frequency, at least to within the width of the laser line and the nonhomogeneous broadening in the system. The reduced photon emission rate combined with the increased phonon emission rate as the barrier narrows should actually further enhance population inversion. However, the reduction in photon emission rate could also reduce gain both by itself and, particularly near threshold, by increasing the relative importance of parasitic dark recombination

mechanisms competing with photon emission that are not sensitive to the final state broadening, such as large angle phonon scattering, carrier-carrier scattering.

V. CONCLUSION

Using the NEGF quantum transport code SEMC, it has been shown that the barrier thickness plays an important role in multiwell quantum lasers not evident via Fermi Golden Rule calculations. In the simple illustrative case considered here, only one barrier and two wells, the GR-based calculations can produce large overestimates in the expected rate of depopulation of the final state for photon emission for relatively thick barriers. Accordingly, sufficiently thin barriers must be maintained to optimize population inversion. Furthermore, as the well thickness is decreased, the increase in homogeneous broadening of the intermediate states associated with their increased depopulation rates reduces the peak photon emission rate. This, in turn, actually further aids population inversion but could ultimately reduce gain in and of itself and by increasing the relative importance of parasitic dark recombination mechanisms. Therefore, in addition to choice of, in particular, the trailing well width as discussed in Ref. 10, the barrier width must be optimized for peak performance, and in a manner not readily apparent through GR-based calculations alone.

ACKNOWLEDGMENT

This work was supported, in part, by the U.S. Army Research Office. M.S. is grateful to Gerald Witt of AFOSR for his encouragement and guidance.

[1] D. Y. Oberli, J. Shah, T. C. Damen, J. M. Kuo, and J. E. Henry, Appl. Phys. Lett. **56**, 1239 (1998).
[2] J. Faist, F. Capasso, C. Sirtori, D. L. Sivco, A. L. Hutchinson, M. S. Hybertsen, and A. Y. Cho, Phys. Rev. Lett. **76**, 411 (1996).
[3] R. Kohler, R. C. Iotti, A. Tredicucci, and F. Rossi, Appl. Phys. Lett. **79**, 3920 (2001).
[4] R. Kohler, A. Tredicucci, F. Beltram, H. E. Beere, E. H. Linfield, A. G. Davies, D. A. Ritchie, R. C. Iotti, and F. Rossi, Nature (London) **417**, 156 (2002).
[5] B. Williams, S. Kumar, H. Callebaut, Q. Hu, and J. Reno, Appl. Phys. Lett. **83**, 5142 (2003).
[6] H. Callebaut, S. Kumar, B. Williams, Q. Hu, and J. Reno, Appl. Phys. Lett. **83**, 207 (2003).
[7] B. Williams, S. Kumar, H. Callebaut, Q. Hu, and J. Reno, Appl. Phys. Lett. **82**, 1015 (2003).
[8] R. Kohler, A. Tredicucci, C. Mauro, F. Beltram, H. E. Beere, E. H. Linfield, A. G. Davies, and D. A. Ritchie, Appl. Phys. Lett. **84**, 1266 (2004).
[9] H. Callebaut, S. Kumar, B. Williams, Q. Hu, and J. Reno, Appl. Phys. Lett. **84**, 645 (2004).
[10] M. A. Stroscio, M. Kisin, G. Belenky, and S. Luryi, Appl. Phys. Lett. **75**, 3258 (1999).
[11] L. F. Register, in *Selected Topics in Electronics and Systems*, edited by Dutta and Stroscio (World Scientific, Singapore, 1998), Vol. 14, pp. 251–279; Int. J. High Speed Electron. Syst. **9**, 251 (1998).
[12] L. F. Register and K. Hess, Appl. Phys. Lett. **71**, 1222 (1997).
[13] L. F. Register, Int. J. High Speed Electron. Syst. **16**, 365 (2000).
[14] L. F. Register, W. Chen, X. Zheng, and M. Stroscio, Int. J. High Speed Electron. Syst. **12**, 1135 (2002).
[15] L. F. Register and K. Hess, J. Appl. Phys. **87**, 303 (2000).
[16] H. Teng, J. P. Sun, G. I. Haddad, M. A. Stroscio, S. Yu, and K. W. Kim, J. Appl. Phys. **84**, 2155 (1998).